EPJ Web of Conferences **84**, 04003 (2015)
DOI: 10.1051/epjconf/20158404003

Autoionizing doubly-excited states of $^3\Sigma_g^-$ symmetry of H_2

F. Argoubi[1,a], M. Telmini[1] and Ch. Jungen[2,3]

[1] LSAMA Departement of Physics, Faculty of Science of Tunis, University of Tunis El Manar, 2092 Tunis, Tunisia
[2] Laboratoire Aimé Cotton du CNRS, Université du Paris-Sud, 91405 Orsay, France
[3] Department of Physics and Astronomy, University College London, London WC1E 6BT, UK

Abstract. We report R-matrix calculations of doubly-excited $^3\Sigma_g^-$ states of molecular hydrogen corresponding to $3\tilde{d}\pi n\tilde{\ell}\pi$ configurations. These states form Rydberg series converging to the $3\tilde{d}\pi$ series limit. They lie in the continuum of the doubly-excited states of $^3\Sigma_g^-$ symmetry built on the $2\tilde{p}\pi$ ion core, and therefore they are autoionized. Calculations of resonance positions and widths are presented.

1. Introduction

It is well-established that doubly-excited states of H_2 play an important role in the dissociative recombination (DR) [1–3] of H_2^+. Such states are ideally described within the framework of multichannel quantum defect theory (MQDT), but in practice many MQDT studies have been hampered by the difficulty to determine the quantum defects directly from first principles, especially when the number of open channels is large and the adjustment of diagonal and off-diagonal quantum defect matrix elements based on experimental data becomes difficult or even impossible. During the last decade, we have been developing the so-called "halfium model" for two-electron molecular systems, which combines the variational R-matrix method with generalized multichannel quantum defect theory implemented in prolate spheroïdal coordinates [4]. The method is designed for the determination of realistic molecular quantum defect matrices from first principles over a wide range of energies and molecular geometries, which should be directly applicable to the calculation of the rovibronic dynamics of higly excited molecular states (dissociative recombination, photoionization, photodissociation). Previous applications ranged from the double-minimum $EF^1\Sigma_g^+$ state at low energy [5] to core-excited states of H_2 of Σ^- symmetry near 27 eV [6].

Notwithstanding any possible role of $^3\Sigma_g^-$ doubly-excited states in the DR process, we are presently involved in a systematic investigation of electronic states of H_2. Here we extend our previous study of $2\tilde{p}\pi n\tilde{\ell}\pi$ Rydberg series to higher energies above the $2\tilde{p}\pi$ threshold and up to $3\tilde{d}\pi$ threshold. In this

[a]Corresponding author: argoubi_fatma@yahoo.fr

energy range, the core excited $3\tilde{d}\pi n\tilde{\ell}\pi\ ^3\Sigma_g^-$ states may autoionize as a result of their coupling with $2\tilde{p}\pi\epsilon\tilde{\ell}\pi$ continua that also have $^3\Sigma_g^-$ symmetry.

After a brief sketch of the "halfium" formalism (Sect. 2) in its updated σ_v-symmetrized version (where σ_v refers to the reflection of the electronic wave function at a plane containing the two nuclei), we present the results of a four-channel calculation that produces quantum defect matrices as functions of energy E and bond length R. Electronic energies and autoionization widths of $(3\tilde{d}\pi)n\tilde{d}\pi$ and $(3\tilde{d}\pi)n\tilde{g}\pi$ ($n \leq 8$) doubly-excited states are reported.

2. R-matrix approach

The variational R-matrix theory of H_2 distinguishes between short-range and long-range interactions of the two electrons, which it treats separately by combining two complementary theoretical tools. Our approach, which at the outset was inspired by the work of Yoo and Greene [7], has been presented in detail in Refs. [4, 6], and only a brief outline will be given here.

The electronic Schrödinger equation is solved first inside a finite ellipsoidal volume for fixed nuclei separated by the internuclear distance R. The variational two-electron basis functions $\overline{y_{ij}}(\vec{r_1}, \vec{r_2})$ are σ_v-symmetrized combinations of functions $y_{i^p j^m}(\vec{r_1}, \vec{r_2})$, which in turn are spin-symmetrized products of one-electron wave functions $\phi_i(\vec{r})$. Thus one writes:

$$\overline{y_{ij}}(\vec{r_1}, \vec{r_2}) = \overline{N_{ij}} \left\{ y_{i^+ j^-}(\vec{r_1}, \vec{r_2}) + (-1)^q\, y_{i^- j^+}(\vec{r_1}, \vec{r_2}) \right\} \tag{1}$$

$$y_{i^p j^m}(\vec{r_1}, \vec{r_2}) = N_{ij} \left\{ \phi_{i^p}(\vec{r_1})\phi_{i^m}(\vec{r_2}) + (-1)^S \phi_{i^m}(\vec{r_1})\phi_{i^p}(\vec{r_2}) \right\}. \tag{2}$$

Here $\vec{r_1}$ and $\vec{r_2}$ are the position vectors of the two electrons, the indices i and j refer to the one-electron wave functions of H_2^+ ion, and $p, m = +/-$. S and q refer, respectively, to the total electron spin and the symmetry of the electronic wave function when the symmetry operation σ_v is applied. $\overline{N_{ij}}$ and N_{ij} are normalization factors. A general variational solution $\overline{\Psi_\beta}(\vec{r_1}, \vec{r_2})$ of the two-electron problem inside the reaction volume is written in terms of the two-electron basis functions $\overline{y_{ij}}(\vec{r_1}, \vec{r_2})$ as [6, 8]:

$$\overline{\Psi_\beta} = \sum_{ij} \overline{c_{ij}^\beta}\, \overline{y_{ij}}, \tag{3}$$

where the index β runs over the variational eigenchannels and the double index ij over the basis set. Each eigensolution $\overline{\Psi_\beta}$ is characterized by a stationary logarithmic derivative with respect to the radial coordiate on the reaction surface $max(\xi_1, \xi_2) = \xi_0$.

Outside the reaction volume the wave function is developed as an expansion over products of target wave functions multiplied by radial functions of the outermost electron. The target wave functions $\Phi_k(E, \omega)$ are defined for each channel k which is represented explicitly in the asymptotic zone. They include in fact all coordinates except the radial coordinate ξ of the outermost electron, that is, they also include the angular part of the latter, and for this reason are often referred to as "surface harmonics". The radial part of the external wave function in turn is written in scattering form, as a linear combination of regular and irregular two-center Coulomb radial functions $f(\xi)$ and $g(\xi)$ for any given total energy E [9]:

$$\overline{\Psi_\beta}(E, \omega, \xi) = \sum_k \Phi_k(E, \omega) \frac{1}{\sqrt{\xi^2 - 1}} \left[f_k(\epsilon_c, \xi)\, I_{k\beta}(E) - g_k(\epsilon_c, \xi)\, J_{k\beta}(E) \right], \tag{4}$$

where ϵ_c stands for the electron energy, within a given channel, with respect to the threshold.

The two forms Eq. (3) and (4) of the solutions $\overline{\Psi_\beta}$ are matched on the reaction surface and thus yield the coefficients $I_{k\beta}$ and $J_{k\beta}$ and hence the short-range reaction matrix $\mathbf{K} = \mathbf{J}\mathbf{I}^{-1}$. The quantum defect matrix $\mathbf{l}(E, R)$ is related to $\mathbf{K}$ according to $\mathbf{K}(E, R) = \tan \pi\boldsymbol{\mu}(E, R)$. Quite often quantum defects turn

out to exhibit smooth variations both with the energy E and with the bond length R, as one might expect for quantities reflecting short-range interactions.

Once the reaction matrix $\mathbf{K}$ is known on an appropriate mesh of E and R values spanning the range of interest, the physical MQDT boundary conditions are applied in order to obtain observable quantities such as bound state positions, cross sections etc. The boundary conditions are cast in the form of a determinant whose zeros are to be found:

$$\det|\tan[\beta_k(E)]\delta_{kk'} + K_{kk'}(E)| = 0, \tag{5}$$

where β_k is the asymptotic phase parameter appropriate for each channel k depending on the channel energy ϵ_k: for $\epsilon_k < 0$ it is equal to the phase accumulated by the oscillating asymptotic radial function before it diverges as $\xi \to \infty$, whereas for $\epsilon_k > 0$ it is equal to the negative of the open-channel eigenphase, $-\pi\tau_\rho$. The N_o eigenphases $\pi\tau_\rho$ (with N_o the number of open channels) are obtained by solving Eq. (5) with $\beta_k(E)$ as stated.

A useful theoretical tool for the analysis of a continuum containing resonant structures is the state density $N(E)$, which is defined by

$$N(E) = \frac{d}{dE}\Big(\sum_\rho \pi\tau_\rho\Big), \tag{6}$$

where the sum is taken over the N_o open channels. In the case of a single closed core-excited Rydberg channel that is only weakly coupled to the continua, $N(E)$ will consist of a Rydberg series of Breit-Wigner profiles centered on the positions of the core-excited Rydberg states, which are readily interpreted in terms of resonance positions E_n and autoionization decay widths Γ_n. Conversely, when the channel interactions are strong and many channels are present, "overlapping" resonances occur, and the concepts of resonance position and width become blurred to some extent. Such a situation was encountered for instance in the $Q_4 \ldots Q_9\,{}^1\Pi_u$ resonances of H_2 studied in an earlier publication [10].

3. Results

The continua $(2\tilde{p}\pi)\epsilon\tilde{\ell}\pi$ of ${}^3\Sigma_g^-$ symmetry present above the $2\tilde{p}\pi$ threshold correspond to *odd* $\tilde{\ell}$, while core-excited Rydberg series of ${}^3\Sigma_g^-$ symmetry associated with the $3\tilde{d}\pi$ ion core state correspond to $(3\tilde{d}\pi)n\tilde{\ell}\pi$ with *even* $\tilde{\ell}$. In the present calculations we have explicitly included four channels in the asymptotic expansion of Eq. (4), namely two continua, $(2\tilde{p}\pi)\epsilon\tilde{p}\pi$, and $(2\tilde{p}\pi)\epsilon\tilde{f}\pi$ and two core-excited Rydberg channels, $(3\tilde{d}\pi)n\tilde{d}\pi$ and $(3\tilde{d}\pi)n\tilde{g}\pi$. Effectively we thus have included all contributing partial waves up to $\tilde{\ell} = 4$.

The calculations have been carried out using a reaction volume parametrized as a function of the internuclear distance R (in a.u.) according to $\xi_0 = 1 + C/R$ [7], with the constant $C = 20$ a.u. chosen such that the energy of the confined core orbital $3\tilde{d}\pi$ deviates from the exact value of the free H_2^+ ion by less than about 10^{-3} a.u. over the whole range of $1 \le R \le 8$ a.u. considered [4]. The variational basis included about 200 "closed" functions (that vanish on the reaction boundary), with two "open-type" basis functions (whose derivative vanishes on the reaction boundary) added for each asymptotic channel. We ascertained in all calculations that the basis was well balanced including roughly equivalent contributions from each asymptotic channel. The quantum defect matrix was evaluated for typically 50 energies on a grid spanning the range between the $2\tilde{p}\pi$ and $3\tilde{d}\pi$ thresholds.

3.1 Density of states

Figure 1 displays the state density $N(E)$ obtained for the range between the $2\tilde{p}\pi$ and $3\tilde{d}\pi$ thresholds and for three different $R-$values as functions of the energy. It may be seen that the $(3\tilde{d}\pi)^2$ and $(3\tilde{d}\pi)4\tilde{d}\pi$ resonances appear well isolated at the low energy end of the spectrum, whereas starting with $n = 5$ the

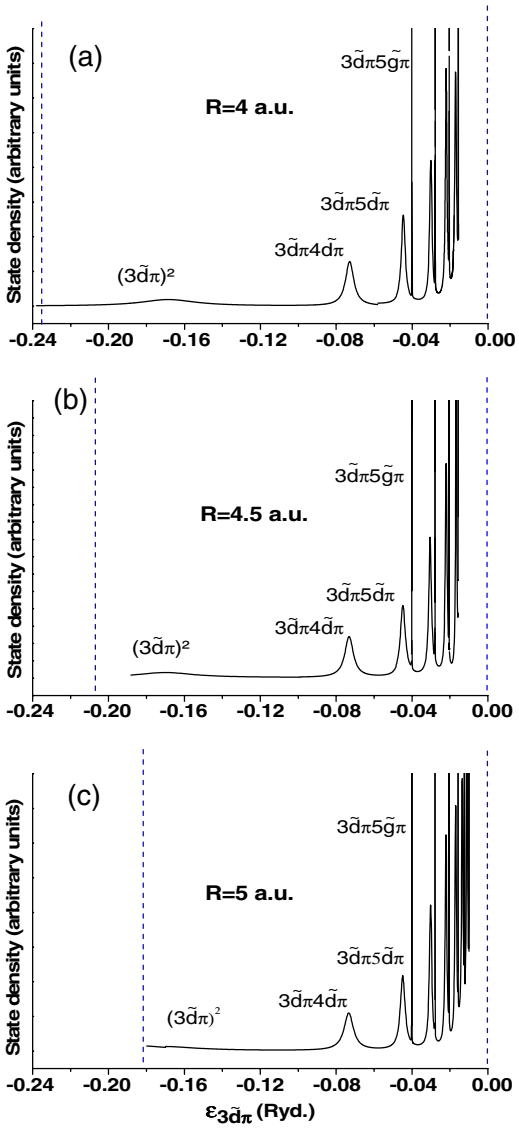

Figure 1. State density plot of $(3\tilde{d}\pi)n\tilde{d}\pi$ and $(3\tilde{d}\pi)n\tilde{g}\pi$ doubly-excited ${}^3\Sigma_g^-$ states of H_2 for internuclear distances (a) $R = 4.0$ a.u., (b) $R = 4.5$ a.u. and (c) $R = 5.0$ a.u.). Energies, in Rydbergs, refer to the $3\tilde{d}\pi$ threshold. The $2\tilde{p}\pi$ and $3\tilde{d}\pi$ H_2^+ ion thresholds are indicated by dashed blue lines.

$n\tilde{d}\pi$ and $n\tilde{g}\pi$ resonances appear as pairs with unequal widths, illustrating how for a given n value the higher partial wave autoionizes much more slowly than the lower one. The three $R-$ values documented by Fig. 1, namely $R = 4.0, 4.5$ and 5.0 a.u., have been selected because they illustrate another interesting phenomenon: it may be seen that the $(3\tilde{d}\pi)^2$ resonance approaches the $2\tilde{p}\pi$ ion threshold from above as R increases, and crosses into the discrete range near $R = 5$ a.u. This is characteristic of an antibonding configuration, and is analogous to the well-known case of the $(2\tilde{p}\sigma)^2\ {}^1\Sigma_g^+$ resonance at much lower energy, which crosses the $1\tilde{s}\sigma$ ion threshold near $R = 2.6$ a.u. and eventually forms the outer well of the discrete $EF^1\Sigma_g^+$ double minimum state of H_2. This latter crossing, and the associated configuration

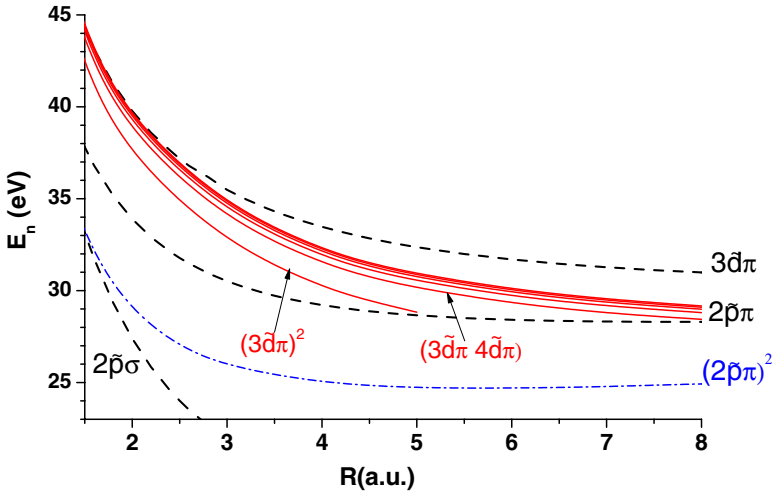

Figure 2. Potential energy curves of doubly-excited ${}^3\Sigma_g^-$ states in H_2: the $(3\tilde{d}\pi)n\tilde{d}\pi$ and $(3\tilde{d}\pi)n\tilde{g}\pi$ autoionizing resonance series are indicated by full red lines. The H_2^+ thresholds $2\tilde{p}\sigma$, $2\tilde{p}\pi$ and $3\tilde{d}\pi$ are represented by dashed black lines. The lowest state of ${}^3\Sigma_g^-$ symmetry, $(2\tilde{p}\pi)^2$ (from [6]), is indicated by the dashed-dotted blue line. The energy scale, in eV, refers to the $X^1\Sigma_g^+$ ground state minimum.

Table 1. Electronic energies (in Rydbergs) of doubly-excited ${}^3\Sigma_g^-$ $(3\tilde{d}\pi)n\tilde{d}\pi$ and $(3\tilde{d}\pi)n\tilde{g}\pi$ states for different internuclear distances R.

State/R (a.u.)	1	2	3	4	5	6	7	8
$3\tilde{d}\pi$	−0.61103	−0.61731	−0.62506	−0.63060	−0.63019			
$4\tilde{d}\pi$	−0.51923	−0.52529	−0.53193	−0.53484	−0.53358	−0.52817	−0.51996	−0.50881
$5\tilde{d}\pi$	−0.49218	−0.49742	−0.50355	−0.50646	−0.50511	−0.49979	−0.49171	−0.48199
$5\tilde{g}\pi$	−0.48712	−0.49343	−0.49942	−0.50199	−0.50035	−0.49521	−0.48772	−0.47889
$6\tilde{d}\pi$	−0.47752	−0.48340	−0.48949	−0.49187	−0.49071	−0.48539	−0.47753	−0.46828
$6\tilde{g}\pi$	−0.47490	−0.48120	−0.48712	−0.48977	−0.48813	−0.48299	−0.47551	−0.46668
$7\tilde{d}\pi$	−0.46858	−0.47532	−0.48115	−0.48396	−0.48229	−0.47709	−0.46941	−0.46023
$7\tilde{g}\pi$	−0.46752	−0.47383	−0.47984	−0.48239	−0.48073	−0.47560	−0.46812	−0.45929
$8\tilde{d}\pi$	−0.46338	−0.47003	−0.47600	−0.47902	−0.47694	−0.47177	−0.46412	−0.45509
$8\tilde{g}\pi$	−0.46274	−0.46904	−0.47508	−0.47759	−0.47593	−0.47079	−0.46331	−0.45449

interaction, is a prototype example of a molecular Rydberg-valence interaction and induces a so-called "direct" DR process.

3.2 Potential energy curves

The resonance positions E_n of the lowest ten doubly-excited states, $(3\tilde{d}\pi)n\tilde{d}\pi$ with $n = 3-8$ and $(3\tilde{d}\pi)n\tilde{g}\pi$ with $n = 5-8$, have been extracted from the state density plots and converted into potential energies in eV. They are shown in Fig. 2 as solid red lines. The $2\tilde{p}\pi$ and $3\tilde{d}\pi$ threshold curves are also represented as dashed black curves. They delimit the energy range of interest here, which varies from 29 to 45 eV. In addition, the doubly-excited state $(2\tilde{p}\pi)^2$, previously studied by Martin [11], Komasa [12] and ourselves [6] is shown as a dotted-dashed blue curve. This state has a minimum at $R = 5.6$ a.u. and may be regarded as a "second ground state" of H_2.

The values of the energies and the effective quantum numbers of the doubly-excited states are given in Tables 1 and 2. As Fig. 2 shows, the potential curves run almost parallel to the $3\tilde{d}\pi$ ion potential,

Table 2. Effective principal quantum numbers n^* of the $(3\tilde{d}\pi)n\tilde{d}\pi$ and $(3\tilde{d}\pi)n\tilde{g}\pi$ resonance series.

State/R (a.u.)	1	2	3	4	5	6	7	8
$3\tilde{d}\pi$	2.470	2.470	2.457	2.435	2.426			
$4\tilde{d}\pi$	3.724	3.730	3.712	3.703	3.692	3.699	3.718	3.776
$5\tilde{d}\pi$	4.711	4.766	4.758	4.738	4.720	4.729	4.761	4.811
$5\tilde{g}\pi$	4.999	4.998	4.996	4.995	4.992	4.992	4.992	4.993
$6\tilde{d}\pi$	5.734	5.774	5.762	5.777	5.728	5.744	5.780	5.822
$6\tilde{g}\pi$	5.999	5.998	5.999	5.991	5.997	5.986	5.986	5.987
$7\tilde{d}\pi$	6.825	6.754	6.776	6.734	6.733	6.740	6.772	6.828
$7\tilde{g}\pi$	7.000	6.996	6.989	6.988	6.984	6.981	6.981	6.983
$8\tilde{d}\pi$	7.840	7.755	7.755	7.645	7.736	7.741	7.780	7.830
$8\tilde{g}\pi$	7.999	7.996	7.978	7.986	7.981	7.978	7.978	7.958

Table 3. Autoionization widths of the resonance series $(3\tilde{d}\pi)n\tilde{d}\pi$ (in units of (10^{-3}) Rydbergs) and $(3\tilde{d}\pi)n\tilde{g}\pi$ (in units of (10^{-6}) Rydbergs).

R	$3\tilde{d}\pi$	$4\tilde{d}\pi$	$5\tilde{d}\pi$	$6\tilde{d}\pi$	$7\tilde{d}\pi$	$8\tilde{d}\pi$	$5\tilde{g}\pi$	$6\tilde{g}\pi$	$7\tilde{g}\pi$	$8\tilde{g}\pi$
1	7.40	1.74	1.44	1.10	0.36	0.18	0.34	0.39	0.26	0.24
2	12.10	5.06	1.50	0.93	0.88	0.67	0.11	0.51	0.49	0.40
3	13.50	3.37	1.74	1.12	0.83	0.55	7.80	2.40	1.30	8.40
4	30.30	4.95	2.32	0.91	0.94	0.90	2.20	2.50	7.40	9.30
5	37.40	5.45	2.94	1.73	1.06	0.72	3.40	3.30	3.20	2.90
6		6.60	3.46	2.40	1.33	0.86	9.30	6.90	5.40	4.20
7		8.80	4.15	2.89	1.60	1.16	22.60	15.60	10.90	7.80
8		14.33	7.38	3.20	1.86	1.27	72.20	54.00	36.20	25.50

indicating that the effective principal quantum numbers vary little with R. This fact emerges clearly from the n^* values shown in Table 2. The corresponding quantum defects are given by $\mu = n - n^*$ and are in fact remarkably constant for $n \geq 4$, as functions of both n and R. Inspection of Table 2 shows that the $\tilde{\ell} = 4$ resonances have very small quantum defects as expected for a non-penetrating outer electron. On the other hand, the quantum defects for $\tilde{\ell} = 2$ are rather large for a $\tilde{d}$ electron in a system with just a few electrons, $\approx 0.25 \pm 0.04$ for $n \geq 4$, and even ≈ 0.55 for the $(3\tilde{d}\pi)^2$ configuration. This behavior reflects the fact that the $n\tilde{d}\pi$ orbitals are penetrating in the present situation because they have a precursor in the core, $3\tilde{d}\pi$ (which is a core orbital of the same symmetry as the series of Rydberg orbitals under consideration). The jump of the quantum defect by a factor of two between $n = 3$ and 4 is related to the fact that for $n = 3$ one has a $(3\tilde{d}\pi)^2$ configuration which is only formally of Rydberg type. Finally, the weak $R-$ dependences of all these series are in sharp contrast with the strong dependences generally found in Rydberg series associated with ground state H_2^+. This in turn appears to be related to the fact that the shape of the core orbital $3\tilde{d}\pi$ changes rather little over the range of R studied here, as compared to the $1\tilde{s}\sigma$ orbital, cf. for instance the contour plots given in the paper by Bates, Ledsham and Stewart [13] (their Figs. 1 and 8).

3.3 Autoionization widths

Table 3 lists the autoionization widths for the $(3\tilde{d}\pi)n\tilde{d}\pi$ and $(3\tilde{d}\pi)n\tilde{g}\pi$ doubly-excited Rydberg series as extracted from the state densities $N(E)$. The widths of the $\tilde{d}$ resonances are seen to be several orders of magnitude larger that those of the $\tilde{g}$ resonances. This is indeed what one qualitatively expects based on the fact that the Rydberg electron with higher $\tilde{\ell}$ penetrates less into the $3\tilde{d}\pi$ ion core. Table 3 further shows that the widths decrease with n – one expects them to decrease roughly proportional to $(n^*)^{-3}$ – and they increase quite significantly with R, in line for what is known in the case of the lower core excited resonances (see e.g. [5], in particular Figs. 5b and 7b).

4. Conclusion

We have presented theoretical energies and autoionization widths of doubly-excited resonances of ${}^3\Sigma_g^-$ symmetry of molecular hydrogen. The energy range between the $2\tilde{p}\pi$ and $3\tilde{d}\pi$ H_2^+ ion thresholds has been explored, from 29 to 45 eV above the H_2 ground state, which is the *lowest-lying* range where Σ^- states are exposed to electronic autoionization. We plan to extend this study to the other molecular Σ^- symmetries.

Ch. J. was supported in part by the ANR (France) under Contract No. 09-BLAN-020901. F. A. and M. T. have received travel support from the same ANR contract. Ch. J. also received funding from the E. Miescher Foundation (Basel, Switzerland).

References

[1] S. L. Guberman, *J. Chem. Phys.* **78** (1983) 1404
[2] A. Giusti, *J. Phys. B. At. Mol. Opt. Phys.* **13** (1980) 3867
[3] I. F. Schneider, O. Dulieu, and A. Giusti-Suzor, *J. Phys. B. At. Mol. Opt. Phys.* **24** (1991) L289
[4] M. Telmini and Ch. Jungen, *Phys. Rev. A* **68** (2003) 062704
[5] S. Bezzaouia, M. Telmini and Ch. Jungen, *Phys. Rev. A* **70** (2004) 012713
[6] F. Argoubi, S. Bezzaouia, H. Oueslati, M. Telmini and Ch. Jungen, *Phys. Rev. A* **83** (2011) 052504
[7] C. H. Greene and B. Yoo, *J. Phys. Chem.* **99** (1995) 1711
[8] S. Bezzaouia, F. Argoubi, M. Telmini and Ch. Jungen, *J. Phys.: Conf. Ser.* **300** (2011) 012013
[9] *see various papers collected in:* Ch. Jungen, *Molecular Applications of Quantum Defect Theory*, Institute of Physics (Bristol) (1996)
[10] H. Oueslati, M. Telmini and Ch. Jungen, *Mol. Phys.* **104** (2006) 187
[11] F. Martin, *J. Phys. B. At. Mol. Opt. Phys.* **32** (1999) L181
[12] J. Komasa, *Phys. Chem. Chem. Phys.* **10** (2008) 3383
[13] D. R. Bates, K. Ledsham, and A. L. Stewart, *Phil. Trans. Roy. Soc.* **A246** (1953) 28